ORIGINAL ARTICLE

European Journal of Applied Physics
www.ej-physics.org

Experimental Investigation of Diffraction caused by Transparent Barriers

Farhad Vedad

ABSTRACT

In addition to wave-particle duality, the contributions of Kirchhoff-Helmholtz are fundamental to the scalar theory of diffraction. The mathematical results of their formulae help predict the maximum intensity of light at the center of the far-field diffraction pattern that coincides with the optical axis. This study demonstrates, via a series of the single-slit experiments, that the Helmholtz–Kirchhoff integral is invalid for transparent barriers. In fact, the experimental results show that the main factors determining the appearance of the diffraction pattern are the refractive index contrast between the barrier and the medium, including the physical invariance of the medium in response to factors such as temperature and pressure, and the dimensions of the barriers.

Keywords: Transparent single-slit experiments, Transparent single-slit experiments, Transparent obstacle experiments, Kirchhoff-Helmholtz integral.

Published Online: September 19, 2020

ISSN: 2684-4451

DOI:10.24018/ejphysics.2020.2.5.19

Farhad Vedad*
Graduate Faculty of Nuclear Engineering and Physics,
Amirkabir University of Technology (Tehran Polytechnic), Iran.
(e-mail: farhad.vedad@gmail.com)

Corresponding Author

I. Introduction

The diffraction of light is one of the most fundamental phenomena in optics. When light passes through a tiny aperture in an opaque diaphragm, diffraction occurs, producing both near-field and far-field measurable effects.

The near- and far-field are termed the Fresnel and Fraunhofer zones, respectively, and the diffraction mechanism is accordingly described by the Fresnel–Kirchhoff and Fraunhofer equations and subsequently by the Helmholtz–Kirchhoff integral [14], [12].

Considering the single slit diffraction in fluid relative to the equivalent experiment in air, if m is the number of a particular dark fringe either side of the zero-order peak, then Y_m is distance of that dark fringe to the center of the diffraction pattern, i.e., the optical axis.

The refractive index of the medium in which the diffraction occurs affects the width of the resulting interference pattern, with a large refractive index leading to a narrower pattern [2], [6]. However, the intensity of corresponding diffraction peaks remains the same (See Fig. 1).

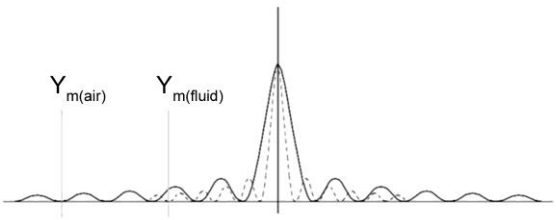

Fig. 1. Single slit diffraction in air (solid line) and water (dashed line).

The width of the diffraction pattern narrows further if the wavelength of the incident light is shortened. In addition, we know that the refractive index of a liquid is larger for the shorter wavelengths.

Typically, the classical concepts of diffraction are considering the behavior of light when it passes through an opaque aperture. On the other hand, most of the experiment with transparent barriers refers to the x-ray beam with the materials that are considered opaque for the visible light. Therefore, the insufficient information about the transparent single slit diffraction causes us to investigate it more.

This article focuses solely on diffraction in the far-field, where the central band is always the brightest, independent of the state of matter of the medium. However, the central band appears different depending on whether a transparent or semitransparent barrier is employed relevantly to the refractive index of the medium.

This study aims to investigate the appearance of the diffraction pattern produced by a transparent aperture in the far-field and subsequently demonstrate that the Helmholtz–Kirchhoff integral is invalid for transparent barriers.

II. Experimental Setup

Measurements were performed using a standard single slit diffraction experimental setup comprising a coherent light source, a single slit aperture, and an observation screen. The performance of a transparent single slit immersed in a selection of liquids at 20 °C was analyzed with respect to its performance in air. As a further comparison, the experiments were repeated at a higher temperature as well.

European Journal of Applied Physics
www.ej-physics.org

Specifically, the dimensions of the far-field diffraction pattern were measured in response to variations in the dispersion of the medium and the size of the aperture.

A convex mirror relevant to the wavelength of the incident light was positioned in the far-field to magnify the diffraction pattern. This allowed the central narrow dark band, which is often very thin, to be observed with the naked eye at larger distances (typically a meter).

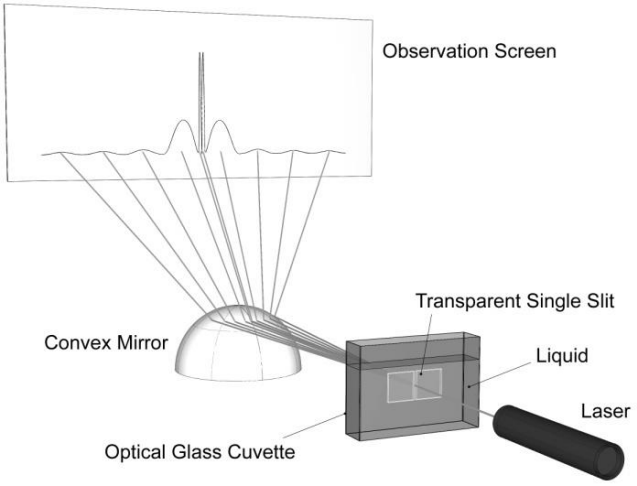

Fig. 2. Transparent single slit diffraction inside a liquid.

The diffraction behavior exhibited by the transparent single slit was examined further via a comparative experiment, for which the transparent slit was replaced by a twin obstacle that comprised two parallel metal strings separated by a narrow gap. This was performed to determine whether the incident laser light interacts with these two different types of barriers in the same manner.

A. Equipment

1) Diode lasers:

450 nm (Polarization Extinction Ratio: 25 dB)
532 nm (Polarization Extinction Ratio: 4 dB)
635 nm (Polarization Extinction Ratio: 20 dB)
780 nm (Polarization Extinction Ratio: 25 dB)
980 nm (Polarization Extinction Ratio: Not Clarified)

2) Transparent single slits:

Glass barriers (n = 1.515) [13] with the following slit widths were employed: 70 µm and 100 µm (thickness =170 µm); 50 µm, 100 µm, and 200 µm (thickness =192 µm); and 100 µm (thickness = 1.0 mm). Furthermore, a borosilicate barrier (n = 1.4714 and it can be 1.474, 1.469, and 1.484 based on the production method. [9]) with a slit width of 100 µm (thickness = 1.1 mm, clear aperture (%): ≥90), sapphire barrier (n = 1.77) [4] with a slit width of 100 µm (thickness =1.0 mm, clear aperture (%): ≥90), and a fused quartz barrier (n = 1.4658 (447.1 nm), 1.4607 (532 nm), 1.4570 (632.8 nm)) with a slit width of 100 µm (thickness = 170 µm, clear aperture (%): ≥90) were used.

3) Opaque single slit:

Metal barrier (302 Stainless steel with black oxide finish) with a slit width of 100 µm (thickness =127 µm).

4) Opaque obstacles:

- Metal string (diameter = 150 µm).
- Twin obstacle (diameter of each string =88 µm; gap between the strings = 100 µm).

5) Transparent obstacle:

- A cuboid glass bar (cross-section of 150 × 150µm, length of 5 mm).

6) Mediums, 20 °C:

- Air; n ≃1.000292 [11]
- Glycerol 61%; n = 1.4145measured sample, (n = 1.414 [3]).
- Glycerol 85%; n = 1.4508 measured sample, (n = 1.4505 [3]).
- Himalayan cedarwood essential oil; n = 1.5070 measured sample, (n = 1.512-1.518 [3]).
- Cassia essential oil (Cinnamomum oil); n = 1.6094 measured sample, (n = 1.5996 at 6 °C, n = 1.5917 at27°C [19]).
-Rapeseed oil (colza oil); n = 1.4705 measured sample, (n = 1.465-1.467 at 20°C [15], 1.470-1.474 at 25°C [18]).
- Aniseed essential oil 100% (Anise); n = 1.5385 measured sample, (n = 1.553-1.557 [8]).
- Benzyl benzoate >99.9% ($C_{14}H_{12}O_2$); n = 1.5681 ([5] and [7]).

7) Sample cell:

- Rectangular optical glass cuvette, path length = 40 mm, width = 100 mm, height = 80 mm.

8) Mirrors:

- Convex mirror, 25mm diameter, 12.5 mm focal length, wavelength range: 700–2000 nm.
- Convex mirror, 50 mm diameter, 25.0 mm focal length, wavelength range: 450–650 nm.

9) Working space:

An eight-meter-long dark room to facilitate photography in the far-field.

III. Experiments

A. Transparent single slit diffraction

The structure of the transparent single slit is the same as that of the ordinary opaque single slit. A transparent single slit comprises two transparent sheets separated by a narrow gap. There are no restrictions regarding the choice of transparent material provided that the transparency through the face of the sheet and the edges is similar. For the experiments performed in this study, glass, borosilicate, sapphire, and fused quartz transparent barriers were employed.

The appearance of a diffraction pattern produced by a transparent aperture is different from that produced by an opaque aperture. This is because, for the far-field case, the point corresponding to the maximum intensity of the light diffracted by an opaque single slit always aligns with the optical axis. However, with a transparent single slit, it is possible that the optical axis will correspond to the point where the intensity of diffracted light is minimum. This behavior cannot be explained using Huygens' Principle;

European Journal of Applied Physics
www.ej-physics.org

moreover, the Fraunhofer and Fresnel–Kirchhoff diffraction equations are no longer valid in this scenario.

B. Transparent straight edge diffraction

Projecting the laser beam onto the straight edge of a glass sheet produces an unusual diffraction pattern: a dark fringe appears at the zeroth order position coinciding with the optical axis. This behavior leads us to consider that the diffraction of light by a transparent single slit will be similar.

Fig. 3 shows the diffraction pattern created by the edge of a microscope coverslip (thickness = 170 μm; n_{glass} = 1.515) irradiated with a 532 nm laser.

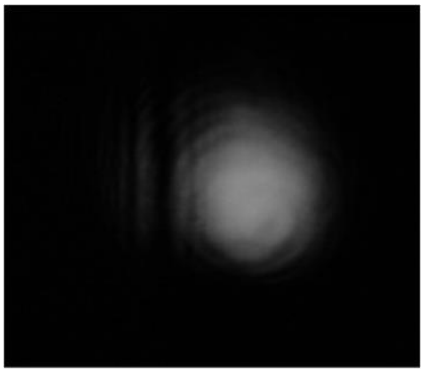

Fig. 3. Glass straight edge diffraction.

C. Single slit diffraction by glass apertures

Figs. 4 and 5 show the single slit diffraction patterns created by a glass aperture with a slit width of 100 μm captured at 10 mm (i.e. the Fresnel zone) and 4 m (i.e., the Fraunhofer zone) distances, respectively. Again, the thickness of the glass barrier is 170 μm. The pattern shown in Fig. 4 has been magnified by a convex mirror; furthermore, it corresponds to a laser wavelength of 532 nm.

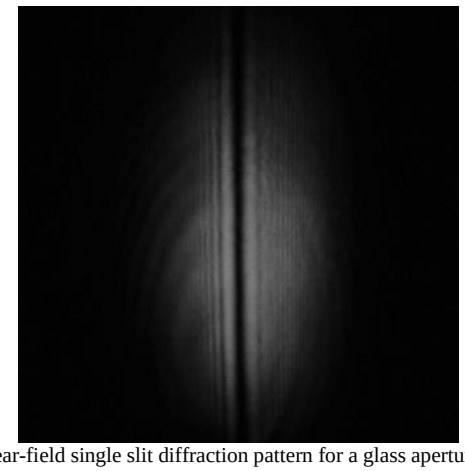

Fig. 4. Near-field single slit diffraction pattern for a glass aperture (width = 100 μm; thickness = 0.17 mm).

Fig. 5 shows the far-field patterns corresponding to 532, 450, and 635 nm. Figs. 4 and 5 illustrate the absence of a constructive interference fringe coinciding with the optical axis.

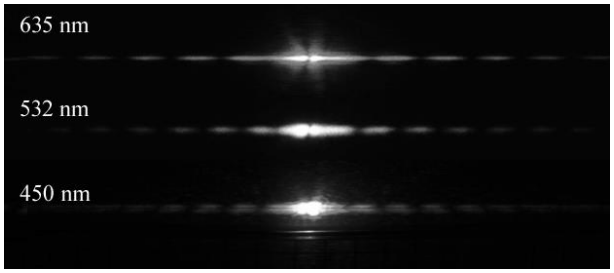

Fig. 5. Far-field single slit diffraction patterns obtained using a glass aperture (width = 100 μm; thickness = 0.17 mm).

While the thickness of the barriers may not change the appearance of the transparent single slit diffraction pattern in either air or a vacuum with respect to the distribution of diffraction fringes, increasing the thickness may attenuate the fringe intensities. Fig. 6 shows the diffraction result for a glass single slit with a width of 100 μm at a distance of 8 m (thickness = 1.0 mm; wavelength = 532 nm). Similarly, this figure shows that the central band on the optical axis corresponds to a destructive interference fringe.

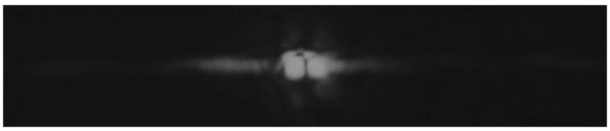

Fig. 6. Far-field single slit diffraction pattern obtained using a thick glass aperture (width = 100 μm; thickness = 1 mm).

Fig. 7 shows the far-field single slit diffraction patterns produced by a glass aperture with a width of 100 μm corresponding to incident wavelengths of 780 nm and 980 nm at a distance of 1.5 m. The patterns are magnified by an infrared convex mirror.

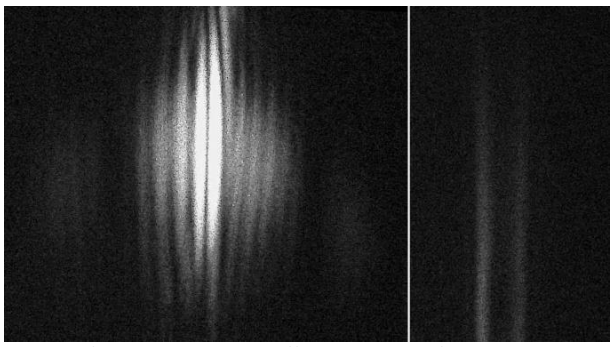

Fig. 7. Far-field glass single slit diffraction patterns for laser wavelengths of 780 nm (left) and 980 nm (right).

Fig. 8 illustrates graphically the general appearance of the far-field transparent single slit diffraction pattern shown in Fig. 5. ΔP is the peak-to-peak distance of the central twin peaks, and ΔP' is the width of the centermost dark fringe.

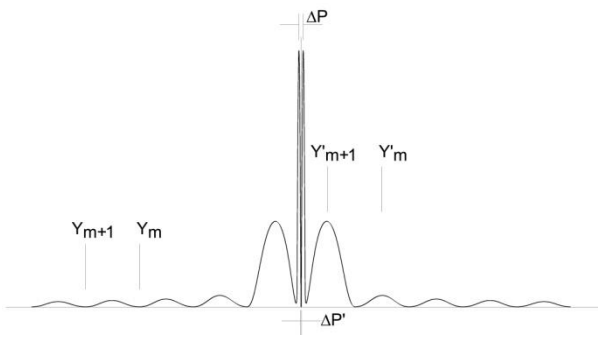

Fig. 8. Schematic of the far-field diffraction by a transparent single slit.

European Journal of Applied Physics
www.ej-physics.org

Applying the wavelength-dependent principles of single slit diffraction by an opaque aperture to the case of a transparent aperture leads to the following relation for 635 nm (red light), 532 nm (green light), and 450 nm (blue light):

$$Y_{m(blue)} < Y_{m(green)} < Y_{m(red)} \quad (3)$$

However, exclusively for a transparent single slit, we obtain:

$$\Delta P_{blue} < \Delta P_{green} < \Delta P_{red} \quad (4)$$

and consequently,

$$\Delta P'_{blue} < \Delta P'_{green} < \Delta P'_{red} \quad (5)$$

It is important to ensure that the edges of the transparent barriers used in the experiments are not frosted, scratched, or coated with an opaque material. If the transparency of the edges is not approximately equivalent to that of the face, then the central dark band may not appear. This effect can be observed using the example of a fused quartz single slit (a slit width of 100 μm and thickness of 170 μm), as illustrated in Fig. 9(a), which shows the single slit diffraction pattern created by a fused quartz aperture at a distance of 8 m with a similar result. Fig. 9(b) shows the single slit diffraction pattern created by a glass single slit (a slit width of 100 μm and thickness of 170 μm) and Fig. 9(c) shows the single slit diffraction pattern created by a metal single slit (a slit width of 100 μm and thickness of 127 μm) at a distance of 8 m.

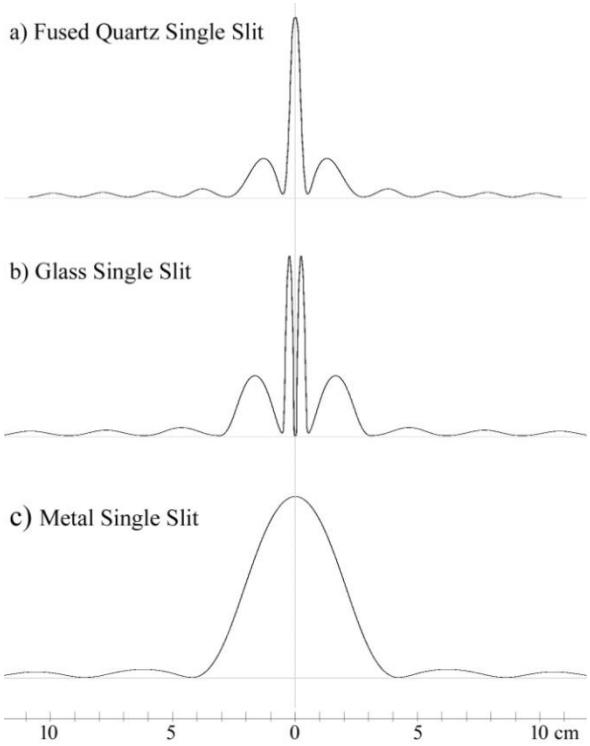

Fig. 9. Schematic of the far-field single slit diffraction pattern for a fused quartz aperture (a), glass aperture (b), and metal aperture (c).

Fused quartz (SiO_2) is a one-component glass formed by melting natural quartz, synthesized quartz, or pure silicate sands at 1700–1800°C. Amorphous (non-crystalline) quartz can be either transparent or opaque. The transparent form is used for optical materials and is known as quartz glass, fused glass, fused silica, or silicate glass. Heraeus HOQ 310 is manufactured by the fusion of natural quartz crystals in an electrically heated furnace that provides an excellent optical transmission that extends from the UV into the IR spectral region [1], [17]. As depicted in Fig. 9, the central band of the diffraction pattern is bright, with the reason for this being that the transparency at the edges of the fused quartz slit is significantly less than that through the center of the barrier, where it is more than 90%.

D. Single slit diffraction by a glass aperture versus diffraction by a twin obstacle

To prove that the edges of the transparent barriers used in the experiments discussed in the previous section are not replicating the behavior expected for a twin obstacle, the setup was modified with a pair of parallel metal strings(with a diameter of 88 μm) separated by a 100 μm gap representing the twin obstacle.

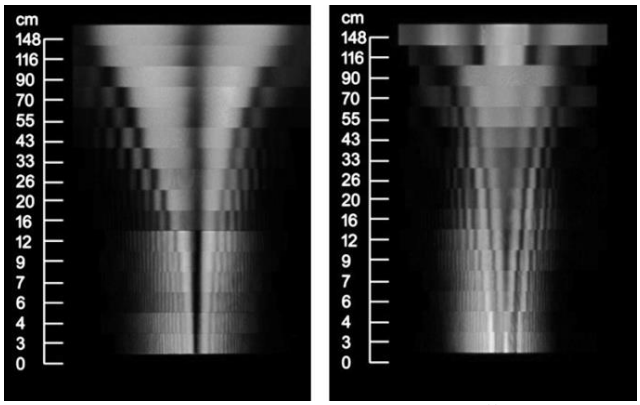

Fig. 10. Logarithmic-scale trajectories comparing the diffraction patterns produced by single slit diffraction from a glass aperture(left) with twin obstacle diffraction from a parallel pair of thin metal wires (right).

The diffraction trajectory patterns, shown in Fig. 10, reveal striking differences between the glass single slit and twin obstacle experiments.

It is possible that the same results will be observed with other transparent materials, including transparent soft plastics.

E. Effect of refractive index on diffraction by transparent single slit apertures

The refractive index of glass is significantly higher than that of air; therefore, single slit diffraction by transparent apertures immersed in liquids with larger refractive indices was considered. Glycerol 61%, glycerol 85%, rapeseed oil, Himalayan cedarwood essential oil, aniseed essential oil(Pimpinella anisum), Cinnamomum oil, and benzyl benzoate were used as liquid media, and transparent apertures made of glass, borosilicate, and white sapphire were used according to the setup outlined in Fig. 2. The refractive index of cedarwood oil is approximately equal to that of glass, and that of rapeseed oil (colza oil) is approximately equal to that of both borosilicate and fused quartz. Thus, the diffraction patterns created using the glass single slit inside cedarwood oil and using the borosilicate single slit inside rapeseed oil can be meaningfully compared. The refractive indices of cedarwood oil and benzyl benzoate are higher than those of borosilicate and glass, respectively. Conversely, the refractive index of glycerol 61% is less than that of borosilicate, and the

European Journal of Applied Physics
www.ej-physics.org

refractive index of rapeseed oil is less than that of glass. Hence, the diffraction patterns corresponding to these material/medium combinations can also be meaningfully compared.

In this section, five conditions for the transparent single slit diffraction are considered:

1- $n_{barriers} > n_{medium}$
2- $n_{barriers} \approx n_{medium}$
3- $n_{barriers} < n_{medium}$
4- $n_{barriers} << n_{medium}$
5- $n_{barriers} >> n_{medium} >> n_{glycerol}$

1) Diffraction pattern with $n_{barriers} > n_{medium}$

This experiment entailed a 1.0 mm thick glass single slit with a slit width of 100 µm immersed in rapeseed oil (n_{glass} 1.515>$n_{rapeseed}$1.4705) and a 1.1 mm thick borosilicate single slit with a slit width of 100 µm immersed in glycerol 61% ($n_{borosilicate}$ 1.4714>$n_{glycerol\ 61\%}$ 1.4145).The observation screen was set at a distance of 5 m from the slits. Borosilicate glass (BOROFLOAT 33), which is composed of silicon dioxide (SiO_2; 81%), boric oxide (B_2O_3; 13%), sodium monoxide and potassium oxide (Na_2O/K_2O; 4%), and aluminum oxide (AI_2O_3; 2%), has an intermediate structure; furthermore, it exhibits properties that are a combination of those of fused quartz and soft glass [9].

For both of these transparent single slits, the diffraction patterns corresponding to blue, green, and red laser wavelengths (450 nm, 532 nm, 635 nm) exhibited the profile shown in Fig. 8, although the spatial parameters of the patterns (ΔP, ΔP', and Y_m) were smaller.

2) Diffraction pattern with $n_{barriers} \approx n_{medium}$

In this experiment, a 1.0 mm thick glass single slit with a slit width of 100 µm, immersed in Himalayan cedarwood essential oil (n_{glass} 1.515 ≈ $n_{cedarwood}$1.5070), and a 1.1 mm thick borosilicate single slit with a slit width of 100 µm, immersed in glycerol 85% ($n_{borosilicate}$ 1.4714 ≈ $n_{glycerol85\%}$ 1.4508), were used. The distance from the slits to the observation screen was 5 m.

Fig. 11 shows the far-field patterns that were produced for three laser wavelengths at a5 m distance, and the pattern is similar for both the samples. Along the optical axis, an intense constructive interference fringe is observed for the red laser light only, and a dark fringe is observed for the blue light. Furthermore, a weak bright zeroth-order fringe state is observed for the green light. Notably, (3), (4), and (5) still hold. Furthermore, the dimensions of ΔP, ΔP', and Y_m are decreasing compared with those in the previous stage.

Observing similar diffraction features along the optical axis is common for equivalent experiments performed with an opaque single slit for both near- and far-field diffraction patterns. However, one key difference is that, while the positions of the maxima and minima representing constructive and destructive interference, respectively, are wavelength-independent for diffraction via an opaque single slit, for a transparent single slit, the interference feature at a certain position is wavelength-dependent.

It is interesting to note that the features as shown in Fig. 11 are exclusive to the fair-field pattern, as the near-field for single slit diffraction by a transparent is too close to the slit aperture to be considered.

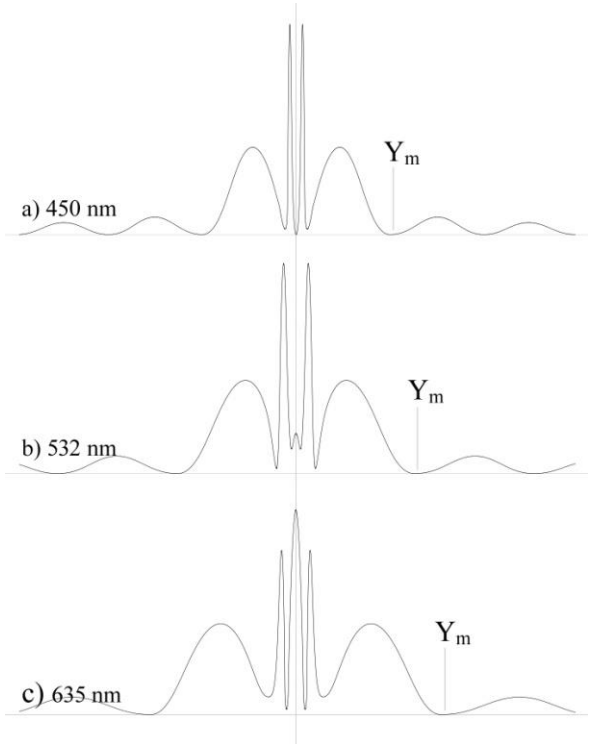

Fig. 11. Far-field transparent single slit diffraction in a medium with a refractive index approximately equal to that of the aperture material.

3) Diffraction pattern with $n_{barriers} < n_{medium}$

It is anticipated that increasing the refractive index of the medium further so that it exceeds that of the aperture will influence the appearance of the diffraction pattern.

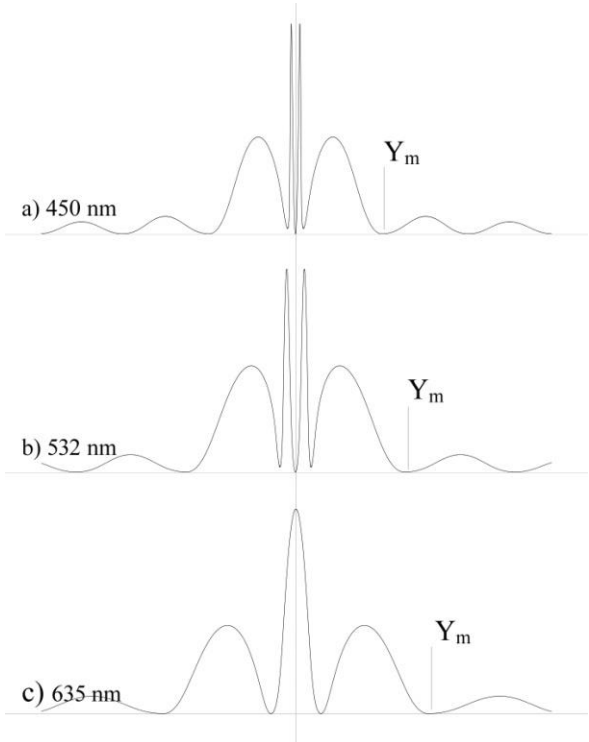

Fig. 12. Far-field transparent single slit diffraction in a medium with a refractive index higher than that of the aperture material.

This variation of the experiment design employed a 1.0 mm thick glass single slit with a slit width of 100 µm, immersed in aniseed essential oil (n_{glass} 1.515 <n_{anise}1.5385), and a 1.1 mm thick borosilicate single slit with a width of 100 µm, immersed in Himalayan cedarwood essential oil ($n_{borosilicate}$ 1.4714<$n_{cedarwood}$1.5070). Again, the distance from the slits to the observation screen was 5 m.

Fig. 12 shows the resulting diffraction patterns, illustrating similar behavior for both samples. The dimensions of ΔP, ΔP', and Y_m are smaller as compared to those in the previous stages (See Fig. 11); in addition, the central bright fringe is larger than those in the previous stages. However, central dark fringes are still observed at wavelengths of 532 and 450 nm.

4) Diffraction pattern with $n_{barriers}$<<n_{medium}

Further increases in the refractive index of the liquid medium relative to that of the transparent aperture result in the loss of the bright fringe coinciding with the optical axis for the red laser light (635 nm), with a dark central fringe being observed for each wavelength investigated, as depicted in Fig. 13. In addition, ΔP, ΔP', and Y_m are significantly smaller than those for the case presented in Fig. 8.

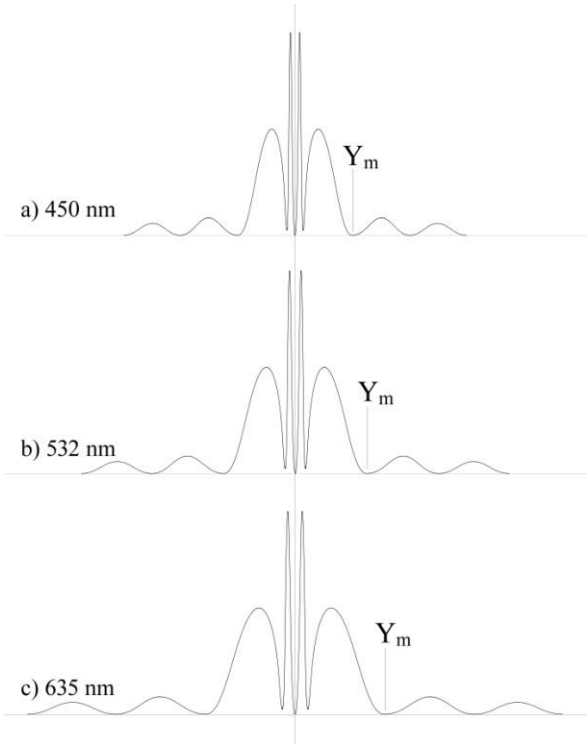

Fig. 13. Far-field transparent single slit diffraction in a medium with a refractive index significantly higher than that of the aperture material.

The diffraction patterns illustrated in Fig. 13 were produced by transparent apertures with the following parameters: a 1.0 mm thick glass single slit with a slit width of 100 µm, immersed in benzyl benzoate (n_{glass}1.515 <<$n_{benzyl\ benzoate}$1.5681), and a 1.1 mm thick borosilicate single slit with a slit width of 100 µm, immersed in aniseed essential oil ($n_{borosilicate}$ 1.4714<<n_{anise}1.5385).

5) Diffraction pattern with $n_{barriers}$>>n_{medium}>>$n_{glycerol}$

The diffraction patterns shown in Figs. 5–7 demonstrate that increasing the refractive index of the liquid medium relative to that of the aperture material affects the appearance of the diffraction pattern, with the spatial parameters ΔP, ΔP', and Y_m steadily decreasing as the refractive index of the liquid medium increases. The smallest value ΔP observed for the experiments described thus far corresponded to the use of benzyl benzoate with a glass single slit.

Next, the refractive indices of both the transparent barriers and the medium were increased further, for example, a 1.0 mm thick sapphire single slit with a slit width of 100 µm immersed in benzyl benzoate ($n_{sapphire}$ 1.77 >>$n_{benzyl\ benzoate}$ 1.5681) was employed.

The resulting diffraction pattern, shown in Fig. 14, indicates that although ΔP and ΔP' are greater relative to those of the equivalent experiment design that employs a glass aperture, Y_m has decreased further.

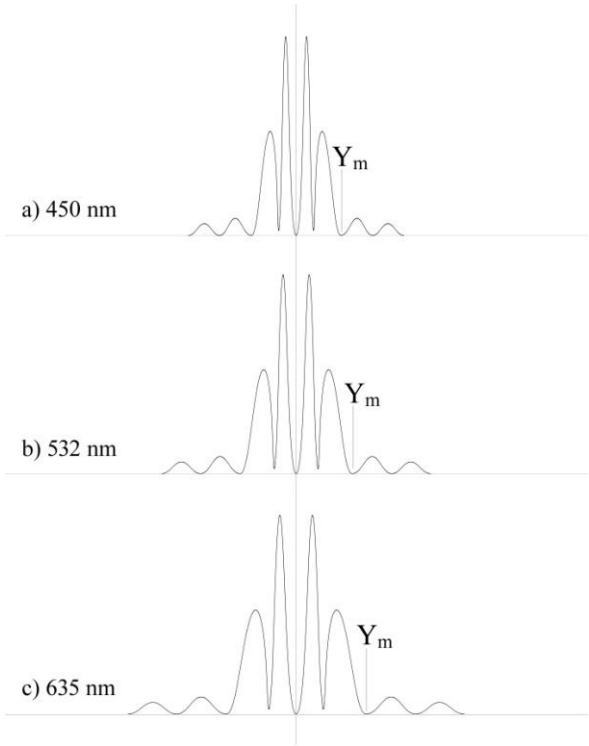

Fig. 14. Far-field diffraction pattern for a sapphire single slit aperture immersed in benzyl benzoate (width = 100 µm; thickness = 1.0 mm).

F. Effect of variable refractive index

The results presented herein demonstrate clearly that the refractive index contrast between the aperture material and the immersion medium is a dominant factor in determining the spatial distribution of the single slit diffraction patterns. This can be distinguished particularly by comparing the example of a fused quartz single slit that the transparency of the edges is not approximately equivalent to that of the face, with glass, transparent soft plastic, borosilicate, and sapphire barriers.

Conversely, this property can be disregarded for the case of opaque aperture diffraction because of the influence of the imaginary refractive index and on the other hand the low refractive index of the medium, especially if the medium is air. This principle was demonstrated via further experiments.

The diffraction pattern corresponding to a 1.0 mm thick glass single slit, with a slit width of 100 µm, immersed in aniseed essential oil at 27 °C is different from that displayed

in Fig. 12(c), showing greater similarity with Fig. 12(b). This is attributed to the decrease in the refractive index as the temperature increases.

An interesting illustrative example for this is provided by immersing a glass single slit in cassia essential oil. Cinnamomum oil is one of the most prevalent organic liquids with a high refractive index of approximately 1.6. The values of the refractive index of Cinnamomum oil obtained for sodium light closely resemble those for daylight. The refractive index is invariant to switching from red (lithium) to green (thallium) light. In response to a temperature variation of 21 °C, the refractive index decreases from 1.5996 at 6°C to 1.5917 at 27°C. Therefore, it is unsuitable for any purpose requiring a medium with constant physical properties. The refractive index of Cinnamomum oil may vary during the experiment, potentially even while the measurement of its refractive index is in progress. Cinnamomum oil consists mainly of cinnamaldehyde (cinnamic aldehyde, $C_6H_5CH{:}CHCHO$), with smaller quantities of cinnamic acid (β-phenylacrylic acid, $C_6H_5CH{:}CHCOOH$). The color of the fresh oil is yellow, but it darkens following exposure to air, turning browner [16], [19]. Consequently, photography with a blue laser becomes difficult. These refractive index inconsistencies were experienced directly while using the green laser, and they were more prominent with the blue laser.

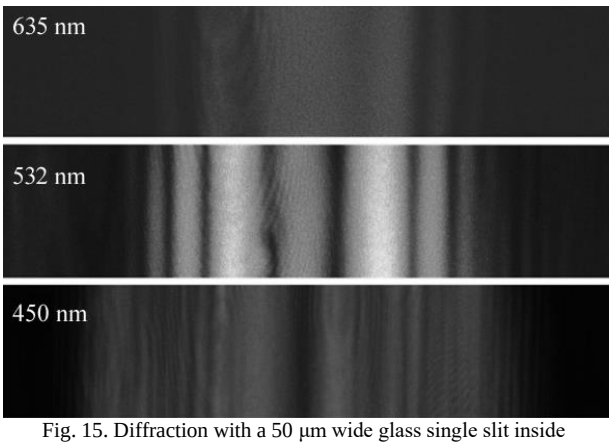

Fig. 15. Diffraction with a 50 µm wide glass single slit inside Cinnamomum oil.

This behavior may cause difficulties while capturing images during the experiment. However, it gradually settles into a steady-state after about two minutes.

As for the glass single slit experiment inside Cinnamomum oil, the diffraction pattern changed rapidly. At times, the central bright band on the optical axis was observed, whereas the dark fringe was observed at other times. The variation was more pronounced at shorter wavelengths and repositioning the laser beam caused the pattern to shuffle; this resembled the changes in the patterns of northern lights. Fig. 15 shows a single slit diffraction pattern for a glass aperture with a slit width of 50 µm immersed in cassia essential oil (n = 1.6094, measured at 20 °C) at the start of the experiment. As Fig. 15 shows, the width of the central bright fringe is larger for the red laser than that for the green laser, whereas it transformed into a dark fringe in the case of the blue laser.

G. Effect of physical dimensions

The other significant factor that determines the form of the diffraction pattern is the physical dimensions of the single slit, including both the thickness of the transparent barriers and the width of the aperture.

The effect of the single slit dimensions was investigated using a 0.192 mm thick glass single slit with slit widths of 50, 100, and 200 µm immersed in rapeseed oil. The distance from the slits to the observation screen was5 m. The 532 nm wavelength laser was used.

Fig. 16 shows that a dark central fringe was observed in the experiments in which 50 µm and 200 µm glass single slits were used, whereas the fringe is bright for an aperture width of 100 µm.

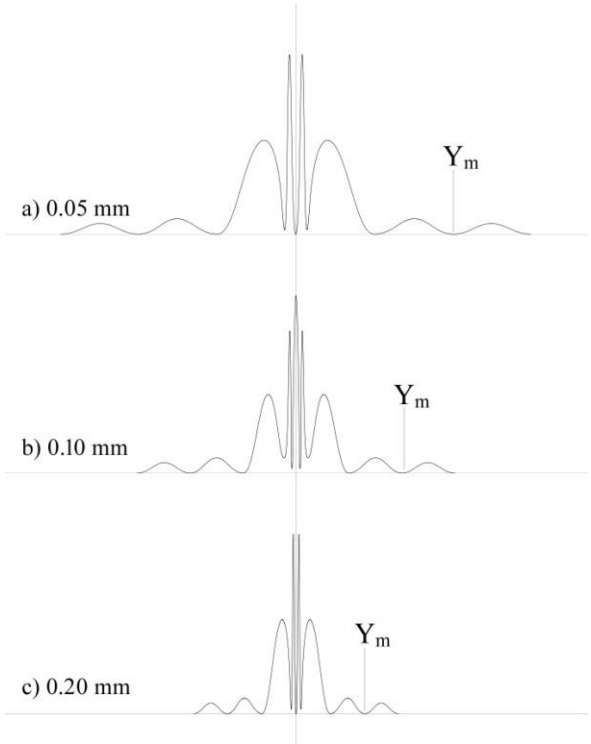

Fig. 16. Far-field single slit diffraction patterns for glass apertures with widths of 50, 100, and 200µmimmersed in rapeseed oil at 27°C.

H. Diffraction due to opaque and transparent obstacles

To augment the study, two further experiments were performed that considered the diffraction due to opaque and transparent obstacles in the far-field. These experiments clarify whether upon encountering an obstacle, light is diffracted in the same manner as that when it encounters a slit.

First, the diffraction pattern produced by a 150 µm metal string in the far-field was imaged. As Fig. 17 shows, the central band on the diffraction pattern has the maximum intensity of light in the far-field (at a distance of 3 m).

To consider the diffraction produced by a transparent obstacle in the far-field, the experiment was repeated with a glass cuboid (cross-section of 150 × 150 µm).

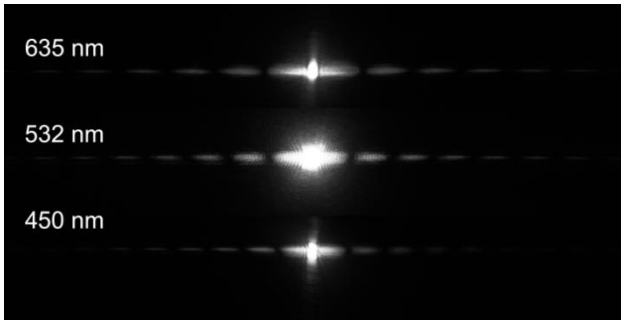

Fig. 17. Far-field diffraction pattern produced by a thin metal string representing an opaque obstacle.

Fig. 18 shows the result of this experiment, which is in similar size and shape to the diffraction pattern observed for an opaque obstacle (at a distance of 3 m) and similar in shape to the diffraction pattern observed for a fused quartz single slit (See Fig. 9). However, the differences become prominent if the pattern is magnified using a convex mirror or short exposure photography. Furthermore, the diffraction pattern observed for a fused quartz single slit with width of 150 μm (at a distance of 3 m) is narrower.

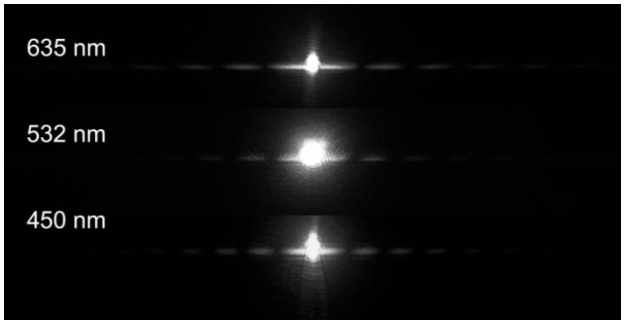

Fig. 18. Far-field diffraction pattern produced by a glass cuboid representing a transparent obstacle.

For the diffraction due to the metal wire, the central bright band maintains its maximum intensity irrespective of the laser wavelength.

Greater variation in the fringe features was observed for the diffraction patterns produced by the glass cuboid. In this case, one key aspect stands out when comparing the long- and short-wavelength patterns: at shorter wavelengths, the intensity of the fringes is diminished with respect to the diffraction pattern produced by a metal string.

IV. Conclusion

In summary, considering the results presented herein, it can be inferred that the main parameter underlying the spatial distribution of the diffraction pattern produced by transparent single slit barriers is the refractive index contrast between the barriers and the medium. In contrast, this quantity can be disregarded for single slit diffraction with an opaque barrier because of the imaginary part of the refractive index of the barriers.

Importantly, it follows that the Fraunhofer and the Fresnel diffraction equations and, consequently, the Fresnel–Kirchhoff diffraction formula are not valid for transparent single slits. This is because the prediction for the central band is constrictive along the optical axis in the far-field, which is not always the case with transparent single slits.

In the case of a transparent single slit, in the far-field, the central band is not always dark. Indeed, its appearance depends on many factors, including the refractive index of the barriers with respect to that of the medium, the physical dimensions of the transparent barriers, and the distance of the observation point. If the edges of the transparent barriers are matte, frosted, or less transparent than the rest of the barrier, then the central band of the diffraction pattern will achieve maximum intensity in the far-field.

Furthermore, the edges of the transparent barriers used in the diffraction experiment are not replicating the behavior expected for a twin obstacle.

References

[1] B. Sakmann and E. Neher, *Single-Channel Recording*. Plenum Press, 1983, pp. 53-57.
[2] C. Denz, Mi. Schwab and C. Weilnau, *Transverse Pattern Form. Photorefractive Opt.* Springer Science and Business Media, 2003, pp. 81-84.
[3] D. Parriott, *A Practical Guide to HPLC Detection*. Academic Press, 2012, pp. 12-20.
[4] E. R. Dobrovinskaya, L. A. Lytvynov and V. Pishchik, *Sapphire: Material, Manufacturing, Applications*. Springer Science and Business Media, 2009, pp. 80-84.
[5] F. Brühne and E. Wright, *Ullmann's Fine Chemicals*, vol. 1. Wiley-VCH, John Wiley & Sons, 2014, pp. 376-377.
[6] F. Zernike and J. E. Midwinter, *Applied Nonlinear Optics*. Courier Corporation, 2006, pp. 1-2.
[7] G. h. Društvo, *Bulletin of the Chemical Society*. Belgrade, vol. 29, no. 5-6, 1964, pp. 5-7.
[8] H. B. Heath, *Source Book of Flavors: (AVI Sourcebook and Handbook Series)*, vol. 2. Springer Science and Business Media, 1981, pp. 220-222.
[9] J. E. Shelby, *Introduction to Glass Science and Technology*. Royal Society of Chemistry, 2005, pp. 266-268.
[10] J. James, *Light Microscopic Techniques in Biology and Medicine*. Springer Science and Business Media, 2012, p. 124.
[11] J. A. Schetz and A. E. Fuhs, *Fundamentals of Fluid Mechanics*. John Wiley & Sons, 1999, p. 202.
[12] K. Klem-Musatov, H. C. Hoeber, T. J. Moser and M. A. Pelissier, *Classical and Modern Diffraction Theory*. SEG Books, 2016, pp. 140-142.
[13] L. Wilson, P. T. Matsudaira, L. S.B. Goldstein and E. A. Fyrberg, Drosophila melanogaster: Practical Uses in Cell and Molecular Biology. Academic Press, 1995, pp. 512-515.
[14] M. Born and E. Wolf, *Principles of Optics*, 7th ed. Cambridge University Press, 1999, pp. 421-439.
[15] M. Bockisch, *Fats and Oils Handbook* (*Nahrungsfette und Öle*). Elsevier, 2015, pp. 257-259.
[16] M. D. Larrañaga, R. J. Lewis, Sr. and R. A. Lewis, *Hawley's Condensed Chemical Dictionary*, 16th ed. John Wiley & Sons, 2016, p. 339.
[17] M. Wakaki, T. Shibuya and K. Kudo, *Physical Properties and Data of Optical Materials*. CRC Press, 2007, pp. 363-371.
[18] N. Board, *Modern Technology of Oils, Fats & Its Derivatives*. India: Asia Pacific Business Press, 2008, pp. 108-109.
[19] W. T. Schaller, "Mineralogical notes", Bulletin 490. United States Geological Survey, Washington: Department of the Interior, series 1, 1911, pp. 60-64.

Farhad Vedad was born in Mashhad, Iran in 1963. After finishing BSc atomic applied physics at Tehran polytechnic university in 1994, he continued environmental engineering for the master's degree. Later he joined the Swedish automotive industry in 1999 and he got Swedish citizenship. Since then, he has worked for several automotive industries in the European countries including BMW, Jaguar Land Rover, and Mercedes-Benz and as Class A Surfacing Senior Manager at Great Wall Motor in China. Now he is working as the senior class A digital surfacing (team leader) at McLaren in the UK.

Mr. Farhad Vedad set up a private physics lab for modern optics and meanwhile he is the author of more than twenty original articles and four

books including "The Maps of Balkhi" which is trying the physics methods to solve a historical geography subject and published by Society for the National Heritage of Iran and the article "Decoding the Secrets in the Story of Bizhan and Manizhe in the Shāhnāme by Using the Methods of Astronomy", published by Uppsala University, Sweden.